2020 IEEE/RSJ International Conference on Intelligent Robots and Systems (IROS)
October 25-29, 2020, Las Vegas, NV, USA (Virtual)

Steering Magnetic Robots in Two Axes with One Pair of Maxwell Coils*

Emma Benjaminson[1], Matthew Travers[2], and Rebecca Taylor[1,3,4]

***Abstract*— This work demonstrates a novel approach to steering a magnetic swimming robot in two dimensions with a single pair of Maxwell coils. By leveraging the curvature of the magnetic field gradient, we achieve motion along two axes. This method allows us to control medical magnetic robots using only existing MRI technology, without requiring additional hardware or posing any additional risk to the patient. We implement a switching time optimization algorithm which generates a schedule of control inputs that direct the swimming robot to a goal location in the workspace. By alternating the direction of the magnetic field gradient produced by the single pair of coils per this schedule, we are able to move the swimmer to desired points in two dimensions. Finally, we demonstrate the feasibility of our approach with an experimental implementation on the millimeter scale and discuss future opportunities to expand this work to the microscale, as well as other control problems and real-world applications.**

I. INTRODUCTION

In this work we introduce a novel approach to steering a magnetic swimming robot in two dimensions using a single pair of Maxwell coils. We move the robot along two dimensions by leveraging the curvature of the field gradient produced by the coils. The authors were inspired by work done in the area of developing medical magnetic swimming robots (also referred to as magnetic swimmers) to implement simultaneous control and imaging in the human body. Medical magnetic swimming robots have been developed to perform tasks such as microsurgical procedures and targeted drug delivery [1], and our proposed solution could be used to perform such tasks using a magnetic resonance imaging (MRI) machine, without requiring any extra hardware or posing any additional risk to the patient. Existing literature suggests that MRI machines are already popular tools for implementing magnetic swimmer procedures in the human body [2]-[6]. We present what we believe is a novel approach that would not only allow the medical community to use magnetic robot technology on patients more easily, but could also be extended to controlling a variety of tools with a reduced number of magnetic field gradients.

*This material is based on work supported by the National Science Foundation under Grant No. 1739308 and by the National Science Foundation Graduate Research Fellowship Program under Grant No. DGE1745016. Any opinions, findings, and conclusions or recommendations expressed in this material are those of the authors and do not necessarily reflect the views of the National Science Foundation.

[1]Department of Mechanical Engineering, Carnegie Mellon University, Pittsburgh, Pennsylvania. Corresponding author: ebenjami@andrew.cmu.edu

[2]Robotics Institute, Carnegie Mellon University, Pittsburgh, Pennsylvania.

[3]Department of Biomedical Engineering, Carnegie Mellon University, Pittsburgh, Pennsylvania.

[4]Department of Electrical and Computer Engineering, Carnegie Mellon University, Pittsburgh, Pennsylvania.

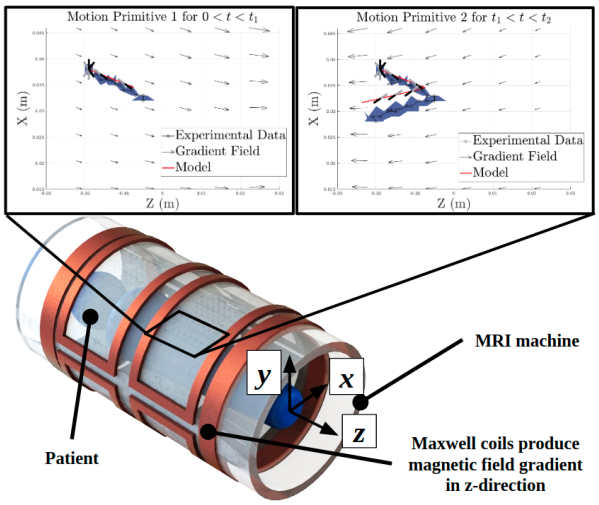

Fig. 1. Control of a magnetic swimming robot is achieved using a single pair of Maxwell coils, representative of the z-axis gradient of an MRI machine. Switching time optimization optimizes the timing of an ordered sequence of control inputs, and the curvature of the gradient field allows for motion in x- and z-directions. As the direction of the magnetic field gradient changes with time (shown in insets), the magnetic swimmer follows the lines of force, which have components in both x- and z-directions.

One of the primary challenges to implementing simultaneous imaging and control with MRI machines is that, if all three pairs of gradient coils must be used to perform both imaging and control, then the coils must frequently alternate between the two functions. MRI machines use magnetic field gradients directed along the three principal axes, x, y and z, to linearly vary the strength of the signal emitted by protons along each direction and thereby encode the position of the signals to form an image [7]-[8]. (See Fig. 1 for orientation of x, y, and z axes used throughout this work.) Rapid changes of the field gradient inside an MRI machine can lead to peripheral nerve stimulation (PNS) in the patient, with symptoms ranging from a mild tingling sensation to serious heart arrhythmia [8]-[10]. One way to avoid inducing PNS in the patient is to reduce the frequency of changes in gradient field configuration, preferably below 100Hz [8]-[9]. However, infrequent images of the magnetic swimmer's location makes it difficult to track a desired trajectory with sufficient precision as is required for most medical procedures [2],[4].

Our solution differs from prior works because we use a single magnetic field gradient produced by the standard MRI configuration of a pair of Maxwell coils fixed in space along the z-axis for steering. We take advantage of the curvature of the z-direction gradient field to achieve nonholonomic motion in both x and z directions simultaneously, as shown in Fig. 1. We move the swimmer in the workspace by alternating

maximum current input to one coil.

The advantage of our solution is that it allows us to simultaneously image and control a swimmer at sufficiently high imaging and command frequencies without approaching frequencies above 100Hz, where PNS is induced [8]-[9]. Recent work has shown that imaging frequencies and control input rates must each be at least 24Hz - 30Hz in order to adequately control swimmers on the macro- [4] and micro-scales [11], respectively. If the same pair of Maxwell coils is used to produce the gradient field required for both imaging *and* control, then the coils would need to change the field at a frequency of approximately $30\text{Hz} \times 2 = 60\text{Hz}$ in order to multiplex the imaging gradient waveform with the control gradient waveform. This 60Hz frequency approaches the limit of 100Hz where PNS is induced. Instead, our proposed solution would separate the imaging functions onto the x- and y-oriented coils, while the z-oriented coils would perform the control function. In this way, each coil could operate in the 30Hz range, allowing for a larger safety margin to avoid PNS.

Given this separation of functions where the x- and y-oriented coils perform imaging and the z-oriented coils apply the control, we optimize the time-varying control fields produced by these coils using switching time optimization. The optimization computes the times at which the direction of the field produced by the z-oriented coils must change, thereby moving the robot to a desired goal location.

In this paper we provide an initial characterization of this method experimentally, and suggest routes for further refinement for both medical purposes and other controls applications.

The key contributions of this work are:

(1) Development of a mathematical model and validation using an experimental setup. An off-line calibration method is also presented to adjust for the individual magnetic swimmer's drag coefficient.

(2) Demonstration of a method of nonholonomic position control with a gradient field produced by a single pair of coils, leveraging switching time optimization in order to move to a goal location.

The rest of the paper proceeds with a review of past work in controlling magnetic robots with MRI machines, and in using switching time optimization for coordinating such control. Then we introduce the theory behind the magnetic field gradients used to propel a magnetic robot, and we present the dynamics model for such a robot, as well as our implementation of the switching time optimization algorithm. We demonstrate our control method with a millimeter-scale robot and discuss our findings. Finally, we present our conclusions and proposals for future work.

II. RELATED WORK

In this section we first review existing methods for controlling magnetic tools with MRI machines, and the additional hardware necessary to do so. We then show how we leverage switching time optimization to develop a novel form of control that would not require any modifications to a standard MRI machine to achieve motion of the magnetic robot in two dimensions.

We will show that our approach is different from prior works because it has a unique combination of features. First, we are able to control a magnetic swimmer in two directions as in prior works, but we are able to do so without making any modifications to the standard hardware used by an MRI machine. Secondly, we are able to simultaneously track and control the swimmer using the MRI machine without approaching the 100Hz threshold of the rate of field gradient changes that induce PNS, as described above. Enabling control in two directions without modifying the hardware, while allowing for simultaneous imaging at frequencies well below the PNS threshold of 100Hz, is unique to our approach, as we will demonstrate in the literature review below.

A. Swimming Robot Control with Magnetic Field Gradients

Recent work on controlling magnetic swimmers with magnetic field gradients can be separated into two categories according to whether the solution used magnetic field gradients generated along two directions or one direction (consider the coordinate system in Fig. 1). The use of gradient fields in two directions has proven to be successful: for example, Steager et al. [11] used two pairs of electromagnets to produce gradient fields in the x and y directions to control micron-scale robots to perform tasks at the cellular level, while imaging with a microscope camera. This work showed that magnetic field gradients can be used to control robots with micron-scale levels of precision. Mathieu and Martel [2], [4] also used magnetic field gradients in two directions to move spherical millimeter-scale magnets through a swine model, alternating between control and imaging with the same MRI machine. These experiments in MRI machines demonstrate that it is possible to achieve two-dimensional control over magnetic swimmers while simultaneously imaging them using only a standard MRI machine [2], [4]. However, there is still a potential danger of inducing PNS in the approach proposed by Martel and Mathieu [2], [4] because as the frequency of changing between control and imaging increases, the likelihood of inducing PNS in the patient increases [8]-[10].

Other researchers have used magnetic field gradients generated along a single axis to control a swimmer. An early example of this approach is the magnetic stereotaxis system developed by Grady et al. [12], which rotated a single coil about a canine's head to move a 5 mm diameter magnet inside its brain. The coil created a magnetic field gradient which provided propulsion while the position of the coil relative to the patient determined the direction of the magnet's motion [12]. Yesin et al. [13] used a similar approach by applying a propulsive force to micron-scale swimmers using a pair of Maxwell coils, while a pair of Helmholtz coils was used to saturate the magnetic material of the swimmers. Steering is achieved by rotating the setup and tracking is performed using a microscope camera [13]. These solutions show that a magnetic field gradient along a single direction is sufficient to propel a swimmer, although

implementing the rotational control over the coils requires the development of additional hardware that is not currently available in common medical tools such as MRI machines.

This section has demonstrated that although there are existing approaches to using MRI machines to control and image magnetic robots, these approaches either require modifications to the hardware, or potentially increase the risk of inducing PNS in the patient. In the next section, we will present switching time optimization and how we use it to develop a control policy that allows for two-dimensional control of magnetic robots with only the coils available in a standard MRI machine.

B. Switching Time Optimization for Steering

Switching time optimization is an appropriate means of optimizing the intervals between a series of control inputs in order to reach a goal location. We assume that we have a fixed set of control inputs where we can alternate turning on and off one coil to some maximum current value. We claim to have a novel application for this existing algorithm, and we will outline the solution to the switching time optimization problem by Johnson and Murphey [14] here.

First, we define the dynamics given in (2) to (4) as per [14], where $\dot{\mathbf{x}} = \mathbf{f}_i(\mathbf{x}(t),\mathbf{u}(t),t)$, $\tau_i \leq t < \tau_{i+1}$. The dynamics, $\mathbf{f}_i$, are represented over the interval $\tau_i \leq t < \tau_{i+1}$ and τ_i and τ_{i+1} are two consecutive switching times. The state of the system is denoted by $\mathbf{x}(t)$ and the control inputs are given by $\mathbf{u}(t)$. Notice that in our situation, the dynamics of the system are fixed and do not change with position or control input; the discontinuity in our system is created by the abrupt change in control inputs $\mathbf{u}(t)$. When the direction of the magnetic field gradient changes abruptly, the swimmer comes to rest instantaneously at the moment of change of control input (because the hydrodynamic drag force acting on the swimmer is significantly larger than the swimmer's inertia), causing a discontinuity in the swimmer's dynamics.

Our objective is to find a series of optimal switching times $\tau_1 \ldots \tau_N$ to optimize a terminal cost, $m(\mathbf{x},t)$. In [14], the cost function is calculated as a running cost because the authors used example applications where the desired trajectory was known. In our case, we only know the goal location so we write our cost function as only the terminal cost, computed at the final time t_f:

$$\begin{aligned} J(\tau_1,\tau_2 \ldots \tau_N) &= m(\mathbf{x}(t_f),t_f) \\ &= \frac{1}{2}(\mathbf{x}(t_f)-\mathbf{x_d})^T(\mathbf{x}(t_f)-\mathbf{x_d}) \end{aligned} \quad (1)$$

where J represents the cost function and we denote the goal location as $\mathbf{x_d}$. We find the optimal switching times by solving a gradient descent problem where we update all of the switching times simultaneously:

$$\tau^{\mathbf{new}} = \tau^{\mathbf{old}} - \alpha \mathbf{H}^{-1}\frac{\partial \mathbf{J}}{\partial \tau}$$

The step size is represented by α and $\mathbf{H}$ is the identity matrix in the case of the first order solution. To obtain the first order derivative of the cost function, we can write it as a product of the costate, $\psi(t_f,\tau_i)$, and $\mathbf{X}^i$, which captures the discontinuities between switching times:

$$\frac{\partial \mathbf{J}}{\partial \tau_i} = \psi(t_f,\tau_i)\cdot \mathbf{X}^i$$

where $\mathbf{X}^i = \mathbf{f}_{i-1}(\mathbf{x}(\tau_i),\mathbf{u}(\tau_i),\tau_i) - \mathbf{f}_i(\mathbf{x}(\tau_i),\mathbf{u}(\tau_i),\tau_i)$. To compute the costate, we can backwards integrate the derivative of the costate from t_f to τ_1. The derivative of the costate given our cost function in (1) is:

$$\frac{\partial}{\partial \tau}\psi(t_f,\tau) = -\psi(t,\tau)\frac{d}{d\mathbf{x}(\tau)}f(\mathbf{x}(\tau),\mathbf{u}(\tau),\tau)$$

The initial condition for the backwards integration of the costate is:

$$\psi(t_f,t_f) = \frac{\partial}{\partial \mathbf{x}(t_f)}m(\mathbf{x}(t_f),t_f)$$

In the next section, we describe how we use this method to obtain a schedule of switching times that allow us to drive a magnetic robot to a goal location using a single pair of Maxwell coils.

III. SYSTEM MODEL AND CONTROL

In this section we will first derive mathematical expressions for the constraints imposed by the environment due to the shape of the magnetic field gradient as well as by the dynamics of the magnetic robot. We will use these expressions to perform model-based control where we will solve for the switching times that drive our robot to a goal location.

A. Magnetic Field Gradient Model

The equations for a magnetic field produced by a pair of Maxwell coils can be written in terms of the vector potential, $\mathbf{A}(\mathbf{r})$ for a single loop of wire carrying a current I as [15]:

$$\mathbf{A}(\mathbf{r}) = \frac{\mu_0 I}{4\pi}\int_0^L \frac{d\mathbf{l}}{||\mathbf{r}-\mathbf{r}'||}$$

where $\mathbf{r}$ is the vector to a point in space, originating from the center of the loop, $\mathbf{r}'$ is the vector from the center of the

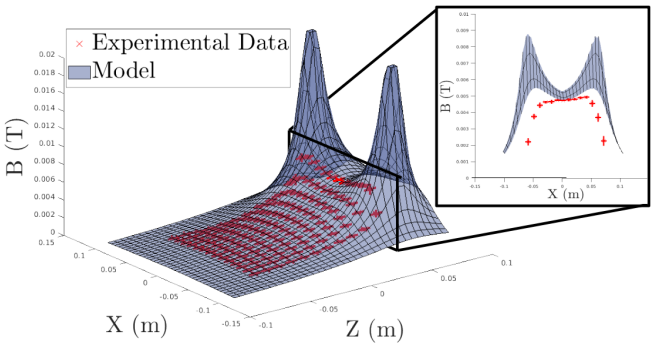

Fig. 2. A comparison of our model of the magnetic field produced by a pair of Maxwell coils with measured field data from our hardware setup. Here, one coil located at z = 0.06m has a current of 1.9A while the second coil has 0 current. Note that the magnetic field values were truncated at 0.02T for the purpose of making the plot easier to read. The measured field data is shown in red with error bars (n = 5 for each data point). Inset compares measured field data to model at z = 0.04m.

loop to a point on the loop circumference, and $d\mathbf{l}$ is a small length component along the circumference of the loop. The vector potential is integrated over the length of the loop, L. The permeability of free space is denoted by μ_0, and the current in the wire is denoted by I.

It is convenient to convert this expression to cylindrical coordinates (represented as ρ, ϕ and z) and rearrange terms to produce the following:

$$\mathbf{A}(\rho,\phi) = \frac{\mu_0 I}{\pi k}\sqrt{\frac{a}{\rho}}\left[(1-\frac{k^2}{2})K(k) - E(k)\right] \text{where}$$
$$k^2 = \frac{4a\rho}{(a+\rho)^2+z^2}$$

$K(k)$ and $E(k)$ are the complete elliptic integrals of the first kind and of the second kind, respectively, and a is the radius of the loop of wire. We can obtain the final expressions for the magnetic field in the ρ and z directions by taking the curl of $\mathbf{A}$ in cylindrical coordinates and writing the expressions for the components of the magnetic field in the ρ and z directions as follows:

$$B_\rho(\rho,z) = \frac{\mu_0 nI}{2\pi}\frac{z}{\rho\sqrt{(\rho+a)^2+z^2}}\left[\frac{a^2+\rho^2+z^2}{(a-\rho)^2+z^2}E(k) - K(k)\right]$$

$$B_z(\rho,z) = \frac{\mu_0 nI}{2\pi}\frac{1}{\sqrt{(\rho+a)^2+z^2}}\left[\frac{a^2-\rho^2-z^2}{(a-\rho)^2+z^2}E(k) + K(k)\right]$$

Note that we have extended this model to account for n turns in a single Maxwell coil. In order to calculate the total magnetic field at a given point, we can add the influence of multiple fields together as $B_i^{total}(\rho,z) = B_i(\rho,z+d) + B_i(\rho,z-d)$ where $i = \rho, z$. Note that the spacing between Maxwell coils, d, is $\sqrt{3}\frac{a}{2}$. The magnetic field described by these expressions for our experimental setup is shown in Fig. 2. The solution presented here focuses on the midplane bisecting the Maxwell coils horizontally, thus the z-axis remains unchanged and the ρ-direction is equivalent to the x-direction.

B. Dynamics of a Single Link Magnetic Swimmer

This work draws inspiration from [16], [17] to derive the equations of motion for a single link swimming robot. We require two reference frames to model the motion of the robot, as shown in Fig. 3. First we have the global frame where we describe the robot's position as $(z,x,\theta) \in R^2 \times S^1$, where z and x are the global positions of the swimmer. The orientation of the tangential axis ($\hat{\mathbf{t}}$) of the swimmer in the global frame is θ. Note that to remain consistent with our magnetic field model above, we use z and x as our position coordinates. Second, we define a body frame fixed to the swimmer's center of gravity. The motion of the body frame is described by $\hat{\mathbf{t}}$ and $\hat{\mathbf{n}}$.

In order to write the equations of motion for the magnetic robot, we can assume that it will accelerate due to the applied magnetic field gradient. Even though the swimmer is in a low Reynolds number environment, the magnetic field gradient will cause the swimmer to accelerate as it approaches a source of magnetic field; this is confirmed

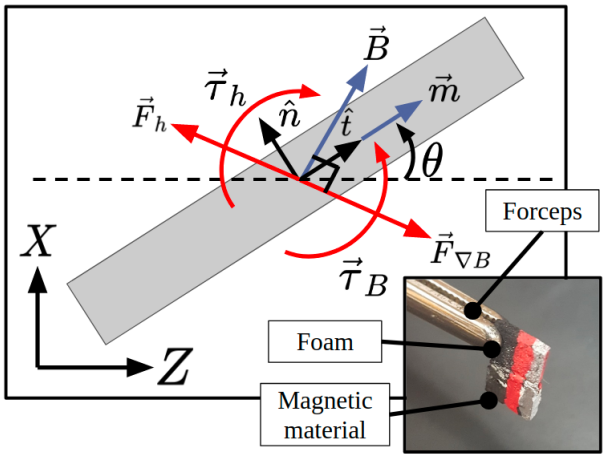

Fig. 3. The single link swimmer sees a combination of forces and torques (red arrows) acting on it from the fluid as well as the externally applied magnetic field (magnetic components shown as blue arrows). $\mathbf{F_{\nabla B}}$ is the magnetic field gradient pulling force on the swimmer, and $\mathbf{F_h}$ is the hydrodynamic drag opposing the motion of the swimmer. $\tau_\mathbf{B}$ is the torque generated by the misalignment between the externally applied magnetic field and the magnetic moment of the swimmer, $\mathbf{m}$. $\tau_\mathbf{h}$ is the hydrodynamic drag torque opposing the rotation of the swimmer. Inset shows the actual magnetic swimmer used in all experiments presented here.

in our experimental results. Therefore, we can write the acceleration of the swimmer in the world frame as follows:

$$\ddot{\mathbf{z}} = \frac{1}{m}(\mathbf{F}_{\nabla Bz} - \mathbf{F}_{hz}) \quad (2)$$
$$\ddot{\mathbf{x}} = \frac{1}{m}(\mathbf{F}_{\nabla Bx} - \mathbf{F}_{hx}) \quad (3)$$
$$\ddot{\theta} = \frac{1}{J}(\tau_B - \tau_h) \quad (4)$$

where m is the mass of the swimmer and we overload notation to represent the robot's rotational inertia as J. The force due to the magnetic field gradient, $\mathbf{F}_{\nabla B}$, can be written as $\mathbf{F}_{\nabla B} = \nabla(\mathbf{m}_B \cdot \mathbf{B})$. We use $\mathbf{m}_B$ to represent the magnetic moment of the swimmer and $\mathbf{B}$ represents the net magnetic field acting on the swimmer at its current location. We assume that the swimmer's magnetic moment is homogeneous throughout its body, given its small size, and that it is aligned with the tangential axis, $\hat{\mathbf{t}}$, of the swimmer.

We assume that the hydrodynamic drag force acting on the swimmer can be calculated as $\mathbf{F}_h = -c_{drag}\mathbf{v}$, where c_{drag} is the coefficient of drag for the swimmer shape in the direction perpendicular to the velocity, $\mathbf{v}$. We define a coefficient of friction for drag acting in the tangential and normal directions, c_t and c_n. Based on resistive force theory [16], [17], we make the assumption that for a long slender body, the drag in the normal direction is twice the drag in the tangential direction. The hydrodynamic drag in the body frame is:

$$\mathbf{F}_h = \begin{bmatrix} -c_t < \mathbf{v}, \hat{\mathbf{t}} > \\ -c_n < \mathbf{v}, \hat{\mathbf{n}} > \end{bmatrix}$$
$$\text{Where } \mathbf{v} = \begin{bmatrix} \dot{z} \\ \dot{x} \end{bmatrix}, \hat{\mathbf{t}} = \begin{bmatrix} \cos\theta \\ \sin\theta \end{bmatrix}, \hat{\mathbf{n}} = \begin{bmatrix} -\sin\theta \\ \cos\theta \end{bmatrix}$$

After calculating the hydrodynamic drag in the body frame, it is possible to decompose it into its components in the

global coordinate frame and incorporate the components into the equations of motion (see Fig. 3 for coordinate frames). The rotational acceleration of the swimmer in the global frame depends on two torques: the torque due to the misalignment between the externally applied magnetic field and the swimmer's magnetic moment, and the torque due to hydrodynamic drag experienced while rotating. We can write the torque due to the magnetic field as $\tau_B = \mathbf{m} \times \mathbf{B}$. Lastly, we can obtain the torque due to hydrodynamic drag by integrating the drag acting over each segment of the swimmer in the normal direction in the body frame. The final expression in the body frame is:

$$\tau_h = -\frac{L^2}{4} c_n \mathbf{v}^T \hat{\mathbf{n}} - \frac{L^3}{12} c_n \dot{\theta}$$

where again we overload notation to say that L is the tangential length of the robot's body. Ultimately, both the magnetic and hydrodynamic torques are acting out of the plane, which has the same direction in both of our coordinate frames so no additional mathematics are required to transform the torques from the local to the global frame.

C. Switching Time Optimization for Steering

The mathematical model for the magnetic field and the swimmer's dynamics can be used to simulate different paths through the fluid. We define one of these paths as a motion primitive, i.e. as the robot's trajectory through the workspace due to the magnetic field gradient created by a single control input for a given time interval. In Fig. 1, we demonstrate how combining two motion primitives can result in a net translation through the workspace.

We use switching time optimization to optimally combine a series of motion primitives together into a trajectory leading to a goal location. To reduce the number of possible control inputs and corresponding motion primitives, we have limited the control inputs to the maximum current (as defined by the coil manufacturer) delivered to one coil at a time. We assume that the order of the sequence of control inputs is known.

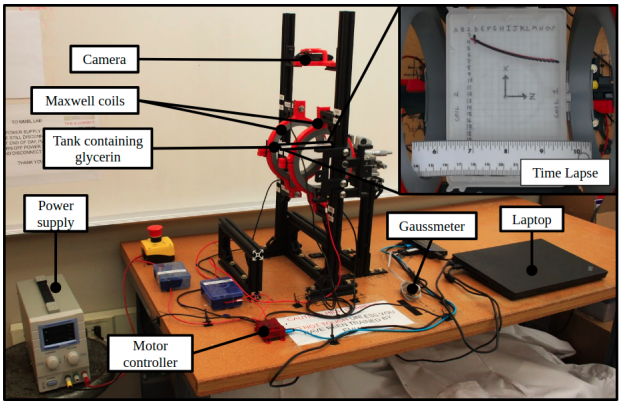

Fig. 4. The experimental setup consists of a pair of Maxwell coils arranged around a container filled with glycerin, which creates a low Reynolds number environment for the magnetic single link swimmer. The coils are powered via a motor controller that modulates current from a power supply. The experiments are recorded by a camera positioned above the workspace. Inset shows a sample time lapse image of motion primitive test.

IV. RESULTS

In this section, we first introduce our experimental setup. Secondly we demonstrate our motion primitives and use the data to obtain the drag coefficient of the robot via gradient descent. Finally, we test our algorithm on two cases: (1) moving the swimmer in one half of the workspace above the z-axis and (2) in the full workspace. Please see our accompanying video for demonstration of these results.

A. Experimental Setup

We use a pair of Maxwell coils (3B Scientific Physics) to generate a magnetic field gradient. The coils receive power from a power supply (Tekpower) via a motor controller (Basic Micro). The coils are arranged around a workspace with a length equivalent to $\sqrt{3}$ of the radius of the coils (this is the defined separation of a pair of Maxwell coils). The workspace is a container filled with glycerin and marked on the bottom with a grid pattern; a ruler is included for scale. A camera (Logitech) positioned overhead records the experiments. The single link swimmer is constructed by mixing an epoxy with a ferromagnetic powder (Magnequench) and cutting the cured material into a rectangular prism of approximate dimensions $3\text{mm} \times 3\text{mm} \times 0.1\text{mm}$. The magnetization of the swimmer is characterized on a vibrating sample magnetometer prior to experimentation. The swimmer is made buoyant by attaching a small piece of foam to the top of the magnetic component and the N and S poles are marked on the swimmer's surface (see Fig. 3 inset).

B. Motion Primitive Tests

We experimentally demonstrated our two motion primitives by sending maximum current to one coil at a time and recording the resultant motion of the robot in the workspace. We processed the videos using ImageJ and the TrackMate plugin [18] to collect the trajectory data, and then used gradient descent to fit our drag coefficient, c_{drag}, to the average trajectory obtained from n = 8 tests for 2 different control inputs. The average trajectory obtained experimentally for a single corresponding control input is plotted against the model's output calculated with the average drag coefficient in Fig. 5.

Although our experimental setup was sufficiently complex for these initial tests, we found some potential areas of

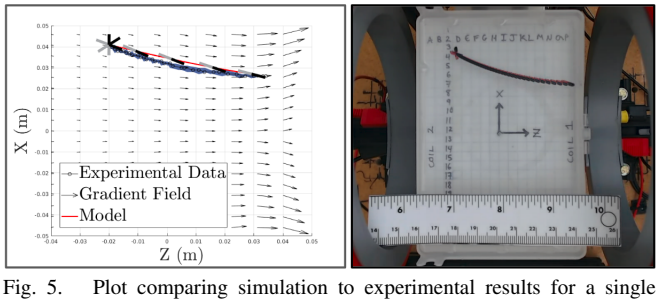

Fig. 5. Plot comparing simulation to experimental results for a single motion primitive. Left: The average of the experimental results obtained from n = 8 test runs is shown with the standard deviation displayed as blue shading around the averaged trajectory. The simulation results are plotted in red for comparison. The magnetic field gradient is also shown as a vector field in the workspace. Right: a corresponding example time lapse image for this motion primitive.

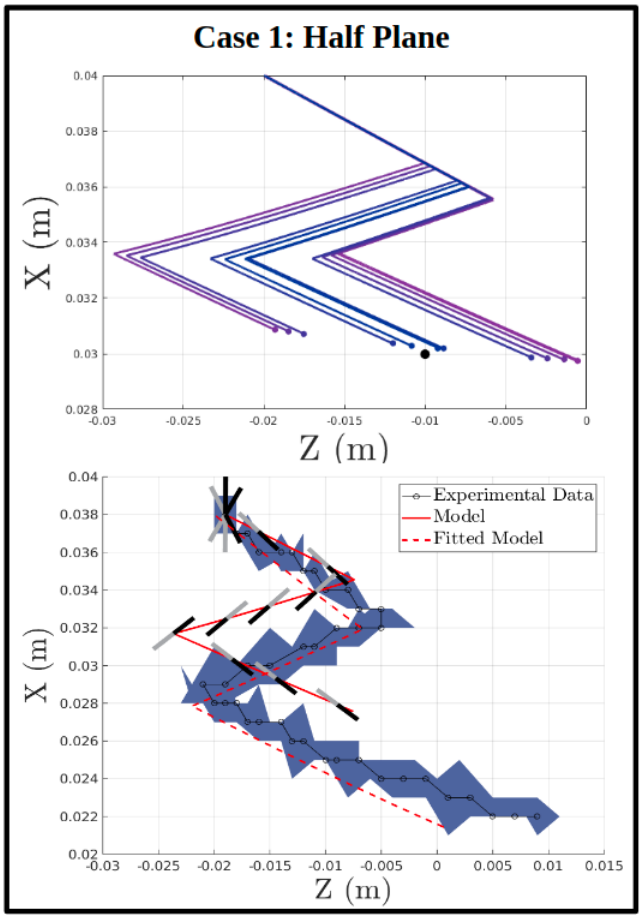

Fig. 6. Model and experimental results for test case 1, moving through one half of the workspace. The start location was (-0.02,0.04)m and goal location was (-0.01, 0.03)m. Top: plot of the progress of our switching time optimization algorithm as it converges on a solution (purple represents early solutions and dark blue represents solutions near convergence). Bottom: experimental results (n = 5) with the model prediction overlaid, using the optimized switching time values. After applying a fitted polynomial to the magnetic field model, we plot the trajectory again, showing improved agreement with the experimental results.

improvement. First, the coils tended to heat up over time; during the 8 test runs, the power drawn by the coils increased by approximately 6% and resulted in a 20% increase in swimmer velocity over consecutive tests. By adding a cooling system to the coils, we could extract excess heat and maintain more uniform performance of the coils. Secondly, our camera and background grid were sufficiently precise to obtain tight standard deviations, as shown in Fig. 5, but they could be improved by adding additional lighting, and a higher resolution camera.

C. Demonstration of Switching Time Optimization

We ran the switching time optimization algorithm presented above on our dynamics model, seeking to obtain the optimal path to move between two points in the workspace. We ran the algorithm on two tuples of start points and goal locations in the workspace. We chose these tuples to test the algorithm's ability to plan a trajectory within one half of the workspace above the z-axis and through the entire workspace, crossing the z-axis. For both of these tests, we show the model's predicted trajectory compared to the experimental results of following the optimized switching times.

In Fig. 6, we see that our switching times did not, experimentally, produce a trajectory that resulted in the swimming robot reaching the goal location. The experimental results (n = 5) showed that the swimmer consistently overshot the goal location. Since we fit our model's drag coefficient to the swimmer using experimental data, we posit that the remaining source of the error is a discrepancy between our model of the magnetic field and the true magnetic field produced by our coils.

To demonstrate that the magnetic field model was the primary source of error in our approach, we overfit to our experimental dataset using a bivariate second-order polynomial to fit our theoretical model to the measured magnetic field (i.e. to the data points illustrated in Fig. 2). We found that the resulting predicted trajectory for case 1 showed better agreement with our experimental results than our purely theoretical model. This is shown in Fig. 6 by the "Fitted Model" curve.

The second test case revealed that we could not cross the z-axis in the workspace, and our model also made this

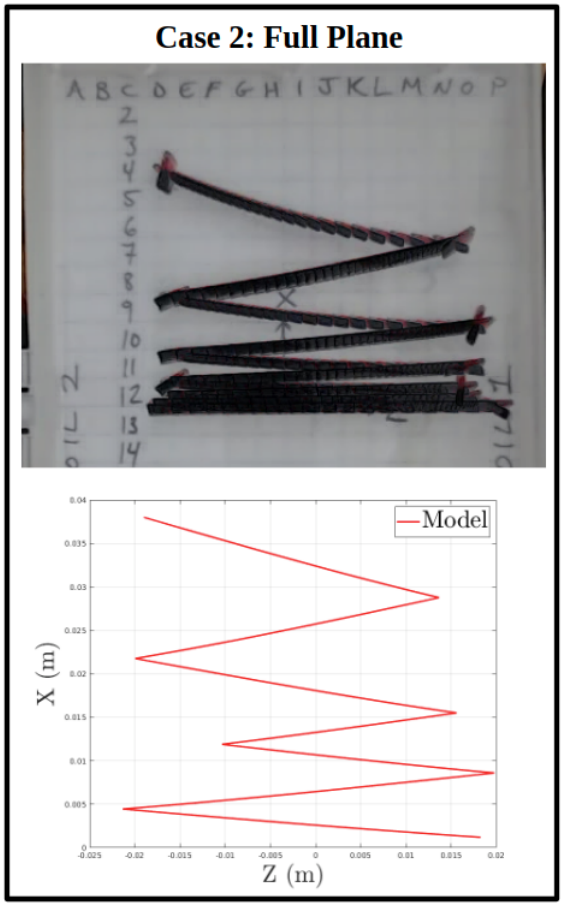

Fig. 7. Top: Time lapse image of test case 2 showing that the magnetic robot cannot cross the z-axis. The lines of force generated by the magnetic field gradient are horizontal at the z-axis, preventing the robot from crossing the axis from above. Bottom: model shows agreement with experimental results.

prediction. In Fig. 7, we can see that as the swimming robot approaches the z-axis, its motion in the x-direction asymptotically decreases. This agrees with our magnetic field gradient model (see Fig. 5), which shows that the lines of force at the z-axis are completely horizontal, so there is no way for the swimming robot to move below the z-axis when approaching from above.

V. CONCLUSIONS

In this work we demonstrated control in two dimensions given an environment with nonholonomic constraints created by the magnetic field gradient from a single pair of Maxwell coils. We used switching time optimization to determine when to alternate between two control inputs to move the swimmer to a goal location in the workspace. We demonstrated that our theoretical approach approximately matched experimental results on the millimeter scale.

The primary advantage of the solution presented here is that it allows for simultaneous imaging and control of a magnetic swimmer in the human body using existing MRI machines without requiring additional hardware, and without increasing the patient's risk of experiencing PNS. In addition, this control approach could be extended to the microscale in order to allow doctors to leverage microswimmer technology in the clinic.

One of the opportunities for future development of this work is to allow for a variable number of control inputs and more flexibility in the control order. Currently, in order to find the optimal switching times, the sequence of control inputs must be known *a priori*. We also believe our switching time optimization approach could be used to solve the problem of simultaneous steering and imaging with an MRI machine another way, by combining the control and imaging gradients in all three axes at appropriate time intervals so that the patient would not be at great risk of experiencing PNS. A potential next step is to implement this solution in an actual MRI machine *in vitro*.

ACKNOWLEDGMENT

The authors wish to thank the following individuals for their contributions: Steven Crews for help with writing a central difference method function in MATLAB; Jaskaran Singh Grover for providing significant mathematical expertise in developing the dynamics model for this work; Andrew Gamble and the Data Storage Systems Center for data on the magnetization of the swimmer; Annie Chen and Daniel Vedova for construction of the experimental setup.

REFERENCES

[1] K. E. Peyer, L. Zhang, and B. J. Nelson, "Bio-inspired magnetic swimming microrobots for biomedical applications," *Nanoscale*, vol. 5, no. 4, pp. 1259–1272, Jan. 2013.

[2] S. Martel, J.B. Mathieu, O. Felfoul, A. Chanu, E. Aboussouan, S. Tamaz and P. Pouponneau, "Automatic navigation of an untethered device in the artery of a living animal using a conventional clinical magnetic resonance imaging system," *Appl. Phys. Lett.*, vol. 90, no. 11, Mar. 2007.

[3] J. B. Mathieu and S. Martel, "Magnetic microparticle steering within the constraints of an MRI system: Proof of concept of a novel targeting approach," *Biomed. Microdevices*, vol. 9, no. 6, pp. 801–808, Dec. 2007.

[4] J. Mathieu and S. Martel, "In vivo validation of a propulsion method for untethered medical microrobots using a clinical magnetic resonance imaging system," *2007 IEEE/RSJ International Conference on Intelligent Robots and Systems*, San Diego, CA, 2007, pp. 502-508.

[5] S. Martel, M. Mohammadi, O. Felfoul, Zhao Lu, and P. Pouponneau, "Flagellated magnetotactic bacteria as controlled MRI-trackable propulsion and steering systems for medical nanorobots operating in the human microvasculature," *Int. J. Rob. Res.*, vol. 28, no. 4, pp. 571–582, Apr. 2009.

[6] J. B. Mathieu, G. Beaudoin, and S. Martel, "Method of propulsion of a ferromagnetic core in the cardiovascular system through magnetic gradients generated by an MRI system," *IEEE Trans. Biomed. Eng.*, vol. 53, no. 2, pp. 292–299, Feb. 2006.

[7] D. Weishaupt, V. D. Kochli, B. Marincek, *How does MRI work? : An Introduction to the Physics and Function of Magnetic Resonance Imaging*. Berlin, Germany: Springer, 2006.

[8] P. M. Glover, "Interaction of MRI field gradients with the human body," *Phys. Med. Biol.*, vol. 54, no. 21, pp. R99-R115, Oct. 2009.

[9] S. S. Hidalgo-Tobon, "Theory of Gradient Coil Design Methods for Magnetic Resonance Imaging," *Concepts Magn. Reson. Part A*, vol. 36, no. 4, pp. 223–242, Jul. 2010.

[10] C. L. G. Ham, J. M. L. Engels, G. T. Van de Wiel, and A. Machielsen, "Peripheral nerve stimulation during MRI: Effects of high gradient amplitudes and switching rates," *J. Magn. Reson. Imaging*, vol. 7, no. 5, pp. 933–937, Sept./Oct. 1997.

[11] E. B. Steager, M. S. Sakar, C. Magee, M. Kennedy, A. Cowley and V. Kumar, "Automated biomanipulation of single cells using magnetic microrobots," *Int. J. Rob. Res.*, vol. 32, no. 3, pp. 346-359, Mar. 2013.

[12] M. S. Grady, M. A. Howard, J. A. Molloy, R. C. Ritter, E. G. Quate and G. T. Gillies, "Nonlinear magnetic stereotaxis: Three-dimensional, in vivo remote magnetic manipulation of a small object in canine brain," *Med. Phys.*, vol. 17, no. 3, pp. 405–415, May/Jun. 1990.

[13] K. B. Yesin, K. Vollmers, and B. J. Nelson, "Modeling and Control of Untethered Biomicrorobots in a Fluidic Environment Using Electromagnetic Fields," *Int. J. Rob. Res.*, vol. 25, no. 5–6, pp. 527–536, May 2006.

[14] E. R. Johnson and T. D. Murphey, "Second-order switching time optimization for nonlinear time-varying dynamic systems," *IEEE Trans. Automat. Contr.*, vol. 56, no. 8, pp. 1953–1957, Aug. 2011.

[15] D. J. Detroye and R. J. Chase, "AD-A286 081 The Calculation and Measurement of Helmholtz Coil Fields", U.S. Army Research Laboratory, Adelphi, MD, ARL-TN-35, Nov. 1994.

[16] J. S. Grover, "Geometric Approaches to Motion Planning for Two Classes of Low Reynolds Number Swimmers," M.S. thesis, Rob. Inst., Carnegie Mellon Univ., Pittsburgh, PA, 2018.

[17] J. Grover, D. Vedova, N. Jain, M. Travers, and H. Choset, "Motion Planning, Design Optimization and Fabrication of Ferromagnetic Swimmers," in *Robotics: Science and Systems, Freiburg im Breisgau, Germany, June 22-26, 2019*, pp. 79 - 88.

[18] J. Schindelin, I. Arganda-Carreras, E. Frise, V. Kaynig, M. Longair, T. Pietzsch, S. Preibisch, C. Rueden, S. Saalfeld, B. Schmid, J.-Y. Tinevez, D. J. White, V. Hartenstein, K. Eliceiri, P. Tomancak, A. Cardona, "TrackMate: An open and extensible platform for single-particle tracking," *Methods*, vol. 115, pp. 80–90, Feb. 2017.